Mechanical and Thermal Properties Enhancement of Polycarbonate Nanocomposites Prepared by Melt Compounding

Sanjay K. Nayak, Smita Mohanty, Sushanta K. Samal

Laboratory for Advanced Research in Polymeric Materials (LARPM), Central Institute of Plastics Engineering and Technology, Bhubaneswar 751 024, India

Received 2 December 2008; accepted 25 July 2009
DOI 10.1002/app.31222
Published online 7 April 2010 in Wiley InterScience (www.interscience.wiley.com).

ABSTRACT: Polycarbonate (PC)/layered silicate nanocomposites were prepared by melt blending technique followed by injection molding from sodium montmorillonite (Na^+-MMT) and a series of organoclay (OMMT-I, Cloisite 20A, and Cloisite15A). The effect of clay types on the mechanical, morphological, and thermal behavior of PC matrix has been investigated. The structure and morphology of the nanocomposites were determined by wide angle X-ray diffraction and transmission electron microscopy. Morphological observation revealed that the organoclay platelets are best exfoliated in PC/Cloisite15A nanocomposites whereas Na^+-MMT clay platelets are poorly dispersed in PC/Na^+-MMT nanocomposites. Differential scanning calorimetry results showed the existence of glass transition temperature (T_g) of PC and the nanocomposites. Thermogravimetric analysis indicated that the increase in onset decomposition temperature of nanocomposites mainly depend on the type of clay and organic modifier. The effect of organoclay on the storage modulus (E'), loss modulus (E''), and damping factor (tan δ) as a function of temperature was measured by dynamic mechanical analysis. © 2010 Wiley Periodicals, Inc. J Appl Polym Sci 117: 2101–2112, 2010

Key words: PC; silicate; morphology; WAXD; DSC; TGA

INTRODUCTION

The study of polymer/layered silicate nanocomposite (PLSN) is currently an expanding field of research as they exhibit wide range of improved properties over their unmodified starting polymers. In principle, small amount of these nanoclays in the range of 3–5% by weight can provide comparable properties as 30–40% by weight of microsized filler do in conventional composites. The improved properties for these nanocomposites include mechanical, thermal, and flammability properties.[1–7] As these nanoparticles are extremely small and their aspect ratios are very high, even at such low loading, the polymer properties can be greatly improved without the detrimental impact on density, transparency, and processibility associated with conventional reinforcements like talc or glass. The performance of the nanocomposites largely depends upon the spatial distribution, arrangement of intercalating polymer chains, and interfacial interaction between the silicate layers and polymers.[8–10] Natural montmorillonite (2 : 1 alumino silicate) (MMT) carries a distribution of negative charges in its inorganic framework so that the framework interacts electrostatically with metal cations present or occurring in its interlayer gallery. Pristine montmorillonite is generally compatible with hydrophilic polymers such as poly (ethylene oxide) whereas it is incompatible with hydrophobic polymers because of its hydrophilic nature. Therefore, the clay is organically modified by replacing interlayer metal cations with various organic cations of onium salts or amines, to facilitate the intercalation of the polymer into the interlayer space between the successively stacked silicate layers. Organic modification lowers the surface energy of montmorillonite by providing such hydrophobic functional groups and improved the interfacial characteristics required to disperse the clay into the matrix.[5,8,11] Melt intercalation of inorganic clay mineral consisting of layered silicates with polymers is widely used, as it is environmental friendly because it does not involve any solvent. Direct polymer intercalation is also the most attractive and viable method because of its low cost, high output, and applicability of current polymer processing.[12] A large number of thermoplastic polymer with varying degree of polarity and chain rigidity have been used as base polymer namely polystyrene,[13] polyamide,[14–16] polyimide,[17] polyurethane,[18] poly (butylene terephthalate),[19] polypropylene,[20–22] polymethyl methacrylate,[23,24] poly (ethylene oxide),[25] poly (4-methyl-1-pentene),[26] and polyacetal.[27]

Correspondence to: S. K. Nayak (drsknayak@yahoo.com).

Polycarbonate (PC) is a transparent amorphous engineering thermoplastic, which exhibits outstanding impact resistance, dimensional stability, heat resistance up to 125°C, higher electrical properties, and excellent clarity, often used to replace glass or metal in demanding applications when the temperature does not exceed 125°C. However, the limitation of PC such as high notch sensitivity, high melt viscosity, and poor chemical resistance needs to improve to extend its engineering application.[28] PC is susceptible to varities of chemical process by thermal and oxidative degradation mechanism at elevated temperature during melt processing.[29–35] PC can be modified and tailored by blending with other polymers for use in demanding applications particularly when its processability and impact strength is important.[36] Researchers[37,38] have made attempts to blend PC with Acrylonitrile-Butadiene-Styrene copolymer (ABS) to modify the properties of PC for commercial application. However, in PC/ABS blend, the interfacial adhesion is not strong due to the immiscibility of PC and styrene acrylonitrile (SAN).[39,40] Seo et al.[41] also reported a continuous decline in the mechanical strength and color change in PC/ABS blend due to the aging of Butadiene rubber in ABS. However, even though a lot of research is done in the field of polymer clay nanocomposites, there is very little work done relating to melt intercalation of PC nanocomposites. Addition of well-dispersed nanofillers to PC could preserve the optical clarity. The transparency, improved stiffness, and scratch resistance make a compelling case for exploring PC nanocomposites, particularly if toughness could also be preserved. Most of the reports on PC/Clay nanocomposites have been based on *in situ* polymerization routes for their preparation including sol–gel process.[42] Zhaobo et al.[43] reported the enhancement in mechanical, morphological, and rheological properties of PC/$CaCO_3$ nanocomposites. Huang et al.[44] reported on PC-layered silicate nanocomposites prepared by two different methods. A partially exfoliated structure was obtained via ring opening polymerization from cyclic oligomers but intercalated layers were obtained via melt mixing in a Brabender mixer using linear PC. Severe et al.[45] studied the thermal stability of PC nanocomposites formed in a twin screw extruder using phosphonium exchanged montmorillonite and synthetic clays. Yoon et al.[46] have studied the effect of organoclay structure on morphology and properties of PC/clay nanocomposites prepared by the melt mixing route. Similarly, Lee and Han[47] reported effect of hydrogen bonding on the rheology of PC/organoclay nanocomposites.

In the present investigation, PC/layered silicate nanocomposites have been prepared by melt intercalation technique. Sodium montmorillonite (Na^+-MMT) and three structurally different organomodified clays (Cloisite 15A, Cloisite 20A, and OMMT-I which prepared in our laboratory by modifying Na^+-MMT with octadecyl trimethylammonium chloride) were taken to evaluate the effect of organically modified montmorillonite on the properties of nanocomposites. A systematic study on the effect of clay loading on mechanical and thermal properties of nanocomposites has been made. The extent of intercalation and dispersion of the clays within the polymer matrix was evaluated using X-ray diffractometer (XRD) and transmission electron microscopy (TEM). The melting, crystallization, and thermal stability of the blend nanocomposites were also studied using differential scanning calorimetry (DSC) and thermogravimetric analysis (TGA). The nanocomposites were also subjected to dynamic mechanical analysis (DMA) to examine the viscoelastic behavior of the materials under periodic stress.

EXPERIMENTAL

Material

Lexan 163(R) PC having density 1.2 kg/m^3 and melt flow index (MFI) of 14.35 g/10 min obtained from LG Polymers India (New Delhi, India) was used as the base matrix. Four types of clays received from Southern Clay Products (India): (i) Natural montmorillonite, i.e., Na^+-MMT (unmodified having cation exchange capacity (CEC) 92.6 meq/100 g), (ii) Cloisite 15A (with the organic modifier dimethyl, dihydrogeneted tallow, quaternary ammonium (2M2HT); CEC 125 meq/100 g), (iii) Cloisite 20A (with the organic modifier dimethyl, dihydrogeneted tallow, quaternary ammonium (2M2HT); CEC 95 meq/100 g), and (iv) OMMT-I (modified Na^+-MMT by octadecyl trimethylammonium chloride, CEC 93.8 meq/100 g). All other chemical reagents were used as received unless otherwise indicated.

Modification of Na^+-MMT by octadecyl trimethylammonium chloride (OMMT-I)

The clay modification was carried out as per the procedure reported by Jisheng et al.[48] Five grams of Na^+-MMT was dissolved in 95 g distilled water under vigorous stirring condition, to form a uniformly dispersed solution. Subsequently, 3 g of octadecyl trimethyl ammonium chloride was added to the solution, which was then stirred for 1 h at 80°C. The dispersed solution was filtered and repeatedly washed with distilled water to remove the excess organic modifier, i.e., octadecyl trimethyl ammonium chloride until there was no white precipitate observed when tested in a 0.1 mol/L $AgNO_3$ solution. The product was then vacuum dried to a

constant weight and ground into powder (diameter about 40–50 μm) to get the organo montmorillonite (O-MMT-I).

Melt compounding

Melt blending of PC and the nanoclays (Na^+-MMT, OMMT-I, Cloisite 20A, and Cloisite 15A) of 1, 3, 5 wt % was carried out in intermeshing counter rotating twin screw-extruder (ctw-100, Haake, Germany) having barrel length of 300 mm and angle of entry 90°. Before extrusion, both polymer matrix and the nanoclays are dehumidified in vacuum oven around 120°C and 60°C for a period of 4 h and 6 h, respectively. The polymer matrix (PC) was fed initially, followed by the organoclay into the molten polymer to avoid clay particles being compacted and not delaminating at a screw speed of 60 rpm, barrel temperature 240°C and the extrudate was pelletized in a pelletizer (Fisons, PP-1, Germany). The melt mixing was performed in a nitrogen atmosphere. The nanocomposites dried and then injection molded using 80T injection molding machine [ESS330/80HL (Engel, Austria) having clamping force 800 KN with a maximum swept volume 254 cm^3 fitted with a dehumidifier (Braid, Germany)] at a temperature 260°C by keeping the mold temperature 90°C at 900 kg/cm^3 injection pressure to prepare tensile, flexural, and impact test specimens as per ASTMD standards. The processing parameter was kept constants for all composition.

Testing and characterization

Mechanical properties

The test specimens of virgin PC and nanocomposites were dried in vacuum at 100°C, kept in sealed desiccators for 24 h before testing. At least three and typically five replicate specimens were subjected to mechanical testing and an average of these measurements was reported. Corresponding standard deviation along with the measurement uncertainty values for the experimental data showing maximum deviation is also included.

Tensile specimens of 165 mm × 13 mm × 3 mm conforming to ASTM-D-638 were strained at a cross head speed of 50 mm per minute and gage length 50 mm in a Universal testing machine (UTM, LR 100K, Lloyds Instruments, UK).

The nanocomposite specimens of dimension 80 mm × 12.7 mm × 3 mm were taken for flexural test under three point bending using the same UTM in accordance with ASTM-D-790, at a cross head speed of 1.3 mm/min and span length of 50 mm.

Izod impact strength testing is an ASTM standard method of determining impact strength. A notched sample is generally used to determine impact strength. For izod impact test, a notch angle of 45° with a V notch depth of 2.54mm was made with a notch cutter on specimens having dimension of 63.5 mm × 12.7 mm × 3 mm. Subsequently, the measurements were carried out in an Impactometer (6545, Ceast, Italy) as per ASTM-D-256.

Morphological Properties

X-ray diffraction. X ray diffractograms of Na^+-MMT, Cloisite 15A, Cloisite 20A, OMMT-I, and the nanocomposites were recorded using Philips 'X'Pert MPD (Japan), X-ray diffractometer unit equipped with nickel filtered Cu Kα radiation source (λ = 0.154056nm) operated at 300 kV and 20 mA. The basal spacing or d_{001} reflection of the samples were calculated from Bragg's equation by monitoring the diffraction angle 2Θ from 2° to 10° at a scanning rate of 2°/min.

Transmission electron microscopy. The nanometer structure of the nanocomposite was investigated using JEOL/JSM, 2000 FX (Begbroke, UK) transmission electron microscope (TEM) with an acceleration voltage of 200 kV. The specimens of 100 nm thickness were cut from the middle section of the injection molded bars in the direction perpendicular to the flow direction using an Reichert Ultracut E microtome (Ontario, Canada) equipped with a diamond knife and placed in a 200-mesh copper grids.

Thermal properties

Differential scanning calorimetry. Perkin Elmer DSC equipment (Diamond DSC) was used to obtain the thermal transition temperature of neat PC and the nanocomposites. The samples were heated from 40 to 200°C at a heating rate of 10°C/min under 30 mL/min of nitrogen atmosphere and kept at this temperature for 5 min before cooling down, to assure that the materials melted uniformly and also to eliminate the previous thermal history. The samples were cooled down to 40°C at the rate of 10°C/min cooling rate followed by a second heating from 40 to 200°C at 10°C/min heating rate. The glass transition temperature (T_g) was detected from the second heating curve.

Thermogravimetric analysis. The thermal stability of the nanocomposites was studied from TGA/DTG curves using Perkin Elmer TGA equipment (Pyris 1 TGA). Samples of ≤5 mg were heated from 50 to 700°C at a heating rate of 10°C/min in nitrogen atmosphere and corresponding weight loss was recorded.

Heat distortion temperature. The heat distortion temperature of the virgin PC and nanocomposites were determined using heat distortion temperature

TABLE I
Effect of Clay Loading on Mechanical Properties

Composition	Tensile strength (MPa)	Tensile modulus (MPa)	Flexural strength (MPa)	Flexural modulus (MPa)	Impact strength (J/m)
PC	70.00 ± 0.81	2350 ± 2.21	90 ± 0.91	2300 ± 1.60	65 ± 0.80
PC+1%Na^+-MMT	76.4 ± 1.10	2532 ± 2.36	99.4 ± 1.21	2511 ± 2.25	43 ± 1.22
PC+3%Na^+-MMT	83.7 ± 0.96	2764 ± 4.23	104.8 ± 0.95	2731 ± 3.10	37.5 ± 1.11
PC+5%Na^+-MMT	81.4 ± 0.96	2610 ± 3.12	101.5 ± 1.10	2665 ± 3.22	31 ± 0.91
PC+1%Cloisite 15A	87.50 ± 0.9	3066 ± 2.23	126.50 ± 0.92	3211 ± 2.26	59 ± 1.10
PC+3%Cloisite 15A	106 ± 1.20	3290 ± 2.54	132.00 ± 0.90	3485 ± 3.20	66.20 ± 0.86
PC+5%Cloisite 15A	99 ± 1.30	3100 ± 3.26	128.00 ± 0.84	3135 ± 4.54	63 ± 0.88
PC+1%Cloisite 20A	86.50± 1.12	2900 ± 4.13	117.50 ± 1.11	2967 ± 4.41	51 ± 1.12
PC+3%Cloisite 20A	98.68 ± 0.86	3115 ± 3.30	127.80 ± 1.23	3235 ± 3.32	57 ± 1.20
PC+5%Cloisite 20A	91.50 ± 0.90	2987 ± 4.28	121.00 ± 1.10	3015 ± 3.27	54 ± 0.92
PC+1%OMMT-I	82.92 ± 1.10	2858 ± 3.39	109.56 ± 1.20	2667 ± 4.10	44.50 ± 0.89
PC+3% OMMT-I	93.6 ± 1.22	3015 ± 2.57	120.80 ± 0.97	2936 ± 3.38	49 ± 0.94
PC+5% OMMT-I	88.54 ± 0.93	2897 ± 4.58	118.15 ± 0.88	2815 ± 2.26	45 ± 0.90

± indicates standard deviation.

equipment Ceast, Italy. The specimens with a dimension of 127 mm × 13 mm × 3.2 mm were studied in accordance with ASTM- D-648 under load of 264 psi.

Dynamic mechanical properties

The dynamic mechanical properties of the nanocomposites were measured by using a DMA–VA–4000 (Germany). The testing parameters were as follows: bending mode, resonant frequency 10 Hz, sample size 35 mm × 12 mm × 3mm, clamping distance, 10 × thickness, static strain 1 Hz, heating rate 10°C/min, and temperature range −150°C to 150°C. In all the cases, four specimens were tested and the average values of storage modulus (E'), loss modulus (E''), and damping factor (tan δ) are reported.

RESULTS AND DISCUSSION

Mechanical properties

Tensile properties

Tensile properties of virgin PC and its nanocomposites with different clays as a function of clay loading in wt % (Table I) were evaluated for the reinforcing benefits of nanoclay in the polymer matrix. It is observed that the tensile strength and modulus increases linearly with the clay loading from 1 to 3 wt %. An increase of ~20% in tensile strength and 18% in tensile modulus in comparison with virgin PC have been obtained with the incorporation of 3 wt % of Na^+-MMT nanoclay. However, the strength and modulus values are lowered for 5 wt % clay loading in comparison to 3 wt %. By examining the clay loading dependence on the tensile properties, it is revealed that the increment in strength and modulus is attributed to the reinforcing characteristics of dispersed nanoclays with high aspect ratio. The decreased tensile properties of the nanocomposites at higher clay loading is due to the filler–filler interaction which results in agglomerates and induced local stress concentration in the nanocomposites and lead to the reduction in the clay aspect ratio thereby reducing the contact surface between the clay and the polymer matrix.[49] Further, the nanocomposites prepared using organically modified clays (Cloisite 15A, Cloisite 20A, and OMMT-I) showed higher strength and modulus as compared to PC/Na^+-MMT nanocomposites. The primary cause for such improvement is probably attributed to the presence of immobilized or partially mobilized polymer phases as a consequence of interaction of polymer chains with organic modification of clays and large number of interacting molecules due to dispersed phase volume ratio characteristics of largely exfoliated nanocomposites.[50,51] Comparing the tensile properties of PC nanocomposites reinforced with Cloisite 15A, Cloisite 20A, and OMMT-I, it is concluded that PC/Cloisite 15A shows optimum tensile performance among all. Tensile strength and modulus of the PC/Cloisite 15A nanocomposites increased to the tune of 27% and 19% as compared with PC/Na^+-MMT which is primarily due to the higher exfoliation of Cloisite 15A having highest CEC value (125 meq/100 g) in PC/Cloisite 15A nanocomposites.

Flexural properties

The variation of flexural properties of the PC nanocomposites along with virgin matrix versus clay loading is summarized in Table I. As observed from the Table I, the flexural strength and modulus shows a similar trend as in the case of tensile properties. The flexural strength of the nanocomposites with

Na^+-MMT clay showed an optimum value at 3 wt % clay loading, beyond which there is a decline in the strength. This behavior is probably due to the presence of clay particles, which possibly acted as stress concentration sites and caused a reduction in the flexural strength of the nanocomposites. Similarly, the flexural modulus of the PC nanocomposites at 3 wt % of Na^+-MMT showed 19% increment as compared with virgin PC. Increase in flexural modulus up to 3 wt % clay loading is attributed to the high stiffness of the nanoclays with aspect ratio acting as plasticizer in nanocomposites. The toughness of the nanocomposites might be decreased because of the nanoparticle clusters inhibiting plastic deformation of matrix by the constraining effect of nanoclay agglomerates as reported to by Rong et al.[52] However, the improvement in flexural properties of the nanocomposites with organomodified clays is more significant than its unmodified counterpart. This behavior might be due to the more plasticizing effect imparted by the organic surfactant used for the modification of Na^+-MMT. It is also observed that the PC/Cloisite 15A nanocomposites exhibited improved flexural strength by 4% and 10% where as the flexural modulus increased to the tune of 8% and 19% as compared to PC/Cloisite 20A and PC/OMMT-I, respectively.

Impact strength

The impact strength of virgin PC and the nanocomposites are also enumerated in Table I. It is evident that the impact strength of the virgin matrix decreased with the incorporation of Na^+-MMT. However, the nanocomposites prepared using organically modified clay Cloisite 15A exhibited nearly same magnitude of impact strength up to 3 wt % loading as that of virgin matrix and beyond that there is deterioration in impact strength. The decline in the impact strength at higher clay loading is probably due to the agglomeration of clay particles, which results in absorbing less impact energy. Similar observations have also been reported by other researches.[53–55] Shah et al.[56] reported that the nanoparticles in the polymer nanocomposites were not allowed to move and hence unable to provide additional energy-dissipating mechanism. The restricted mobility of the nanoparticles in the nanocomposites can initiate crack formation and ultimately led to somewhat brittle behavior.

Comparison of tensile, flexural, and impact properties

A comparative analysis in tensile strength, flexural strength, impact strength and tensile modulus, flexural modulus of virgin PC, as well as the nanocomposites, has been carried out. It is observed that Cloisite 15A-based PC nanocomposites shows optimum mechanical performance as compared to others. The mechanical properties of the nanocomposites is of the order PC/Cloisite 15A > PC/Cloisite 20A > PC/OMMT-I > PC/Na^+-MMT. This behavior is ascribed to the relatively higher dispersion of Cloisite 15A because of its highest CEC (125 meq/100 g) and *d*-spacing (29.45 Å). It can also be noted that even though Cloisite 15A and Cloisite 20A have same type of surfactant (2M2HT: dimethyl, dehydrogenated tallow, quaternary ammonium), Cloisite 15A-based nanocomposites have superior mechanical properties than Cloisite 20A nanocomposites due to higher *d*-spacing and CEC value (*d*-spacing and CEC of Cloisite 20A are 95 meq/100 g and 24.52 Å, respectively). The higher CEC of the clays are inductive to the interaction of the intercalating agent because the higher CEC of the clay exhibit higher Na^+-MMT concentration at the same weight whereas nanoclay with high *d*-spacing allows more amount of polymer matrix to enter into the clay galleries. Higher concentration of modifier on 15A also reduces the moisture uptake as compared to Cloisite 20A resulting in higher mechanical properties. However, basal spacing of Cloisite 20A (24.52 Å) and OMMT-I (22.64 Å) are close to each other, the basal spacing of PC/Cloisite 20A nanocomposites (40.15 Å) is significantly higher than that of PC/OMMT-I nanocomposites (33.92 Å) which indicates higher dispersion of Cloisite 20A as compared with OMMT-I. Basal spacing of organoclay is not only the key factor but also the interaction or miscibility between the matrix and organoclays have plays an important role.[57] Therefore, the good miscibility PC and Cloisite 20A nanocomposites may lead to a higher impact strength performance over OMMT-I. The optimum impact strength of PC/Cloisite 15A may be due to the proper wetting of functional surface of Cloisite 15A with PC matrix.

Morphological properties

Wide angle X-ray diffraction

The wide angle X-ray diffraction (WAXD) results of nanoclays (Na^+-MMT, OMMT-I, Cloisite 20A, and Cloisite 15A) and all the nanocomposites (PC/Na^+-MMT, PC/OMMT-I, PC/Cloisite 20A, and PC/Cloisite 15A) are shown in Figures 1(a–d) and 2(a–d), respectively. The angle of diffraction peak with corresponding d_{001} spacing of the nanoclays and the nanocomposites were also enumerated in Table II. The diffraction peak angle for Na^+-MMT was obtained at $2\Theta = 7^\circ$, which corresponds to interlayer *d*-spacing of 12.6 Å whereas for OMMT-I, Cloisite 20A, and Cloisite 15A, the interlayer *d*-spacing was

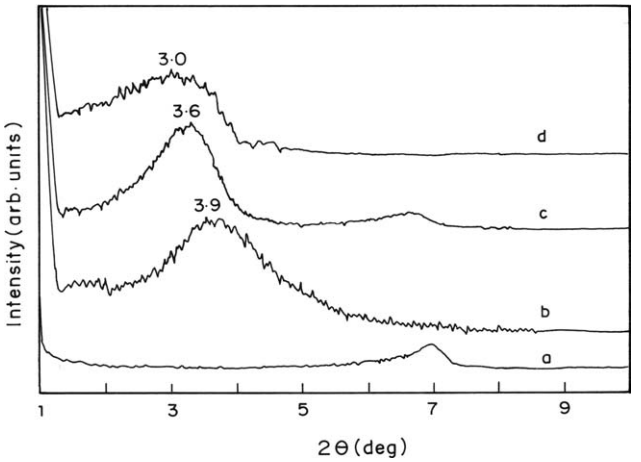

Figure 1 XRD of (a) Na^+-MMT, (b) OMMT-I, (c) Cloisite 20A, (d) Cloisite 15A.

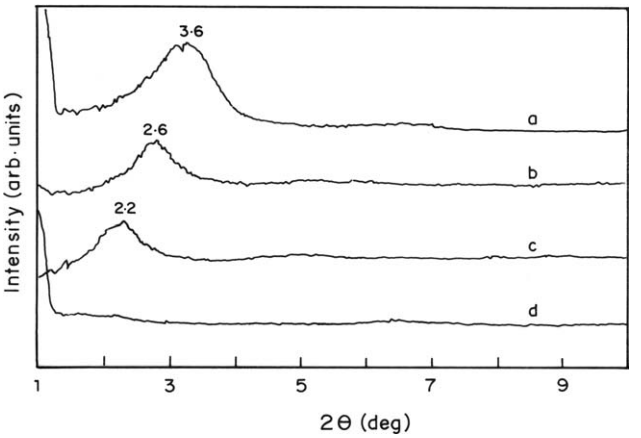

Figure 2 XRD of (a) PC/Na^+-MMT, (b) PC/OMMT-I, (c) PC/Cloisite 20A, (d) PC/Cloisite 15A nanocomposites.

observed at 22.64 Å, 24.52 Å, and 29.45 Å, respectively. Further, it is observed from the Figure 2 and Table II that in case of PC/Na^+-MMT nanocomposites [Fig. 2(a)], diffraction peak shifted to a lower angle ($2\Theta = 3.6°$) as compared to Na^+-MMT, which corresponds a *d*-spacing of 24.52 Å indicating an interacted nanostructure of PC/Na^+-MMT nanocomposites. In this case, PC could not have properly intercalated into pristine montmorillonite which may therefore have resulted in little dispersion of the Na^+-MMT clay stacks in the PC matrix relative to the tightly stacked and much longer range order in the case of Na^+-MMT. However, the results given in Table II showed the 2Θ values of PC/OMMT-I, PC/Cloisite 20A are 3.6° and 2.2° which corresponds to a *d*-spacing of 33.92 Å and 40.15 Å, respectively, indicating the existence of both intercalated and exfoliated nanomorphology.[8,11] However, the absence of diffraction peak of PC/Cloisite 15A nanocomposite clearly indicates exfoliated nanomorphology in which maximum amount of PC matrix are entered interlayers of the Cloisite 15A. The intercalation of Cloisite 20A and OMMT-I compared to Cloisite 15A indicates lower extents of favorable intercalation of Cloisite 20A and OMMT-I with the PC.

TABLE II
Values of Diffraction Peaks and Corresponding *d*-Spacing of Nanoclay and Nanocomposites

Sample	Angle (2Θ)	d_{001}(Å)
Na^+-MMT	7	12.62
OMMT-I	3.9	22.64
Cloisite 20A	3.6	24.52
Cloisite 15A	3	29.45
PC+3% Na^+-MMT	3.6	24.52
PC+3% OMMT-I	2.6	33.92
PC+3% Cloisite 20A	2.2	40.15
PC+3% Cloisite 15A	–	–

This behavior is mainly due to the higher CEC value of Cloisite 15A (125 meq/100 g) as compared to Cloisite 20A (95 meq/100 g) and OMMT-I (93.8 meq/100 g). In the case of PC/Cloisite 15A and PC/Cloisite 20A, even though the organic modifier are same (dimethyl, dihydrogeneted tallow, quaternary ammonium, both ditallow), amine grafting density (equivalent to CEC) was higher (125 meq/100 g) than Cloisite 20A (95 meq/100 g) and grafting density per unit area of the clays is higher by a factor of 125/95 = 1.32. The peaks from XRD studied for all of the intercalated systems were narrow, indicating a high stacking order of the successive clay layers in the hybrid matrix. The strong Bragg diffraction peaks reflected coherent stacking of the clay plate platelets and, thus, the presence of an order structure in the hybrid.

Transmission electron microscopy

TEM can further validate and complement the results of WAXD. TEM micrographs of PC/Na+MMT, PC/OMMT-I, PC/Cloisite 20A, and PC/Cloisite 15A nanocomposites with 3 wt % of nanoclays are presented in Figures 3–6, respectively, where the dark areas represent the clay and the gray/white areas represent the PC matrix. It is clearly seen that in case of PC/OMMT-I, PC/Cloisite 20A, and PC/Cloisite 15A nanocomposites (Figs. 4–6) the organoclay aggregates has been dispersed fairly well with exfoliated nanomorphology which indicates that organic surfactant have played a major role in dispersing the organoclay aggregates. Higher the dispersion of the organoclay aggregates, larger will be the surface areas of the silicate layers of organoclay that become available for specific interactions (i.e., hydrogen bonding) with the carbonyl groups in PC, which in turn increases the degree of dispersion (or exfoliation) of organoclay aggregates. This well-

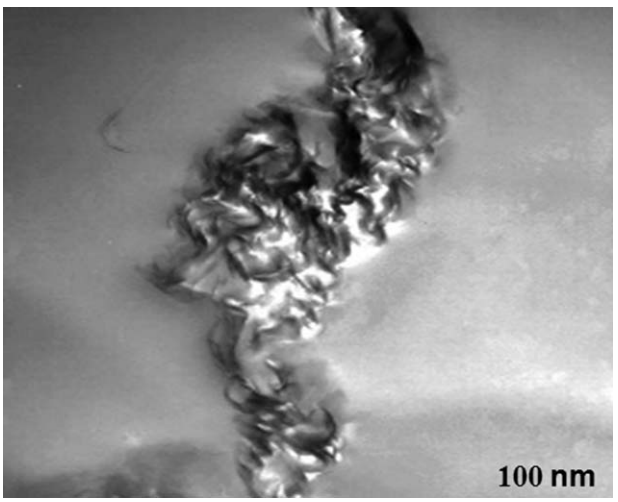

Figure 3 TEM image of PC + 3% Na^+-MMT nanocomposite.

dispersed exfoliated morphology is attributed to the modification of clay with onium salt which lowers electrostatic interaction between the clay layers, enlarged their intragallery spacing thus facilitating exfoliation and efficient dispersion of the clay.[53,58] The average particle size and their corresponding aspect ratio were determined by TEM from the dimensions of ~50 particles is displayed in Table III. In case of PC/Na^+ MMT nanocomposites, the dispersion of the clay particles was poor and many large aggregates of natural clay (in microns) are found to bundle together. However, there are also a large number of individual clay particles which are smaller than this agglomerate. This confirms that the polar interaction between the matrix polymer and Na^+MMT clay would conglomerate to form large aggregate. However, in case of PC/Cloisite 15A nanocomposite, the Cloisite 15A layers dispersed in the matrix is about 162 nm length and 3 nm thickness corresponding to a highest aspect ratio of 54

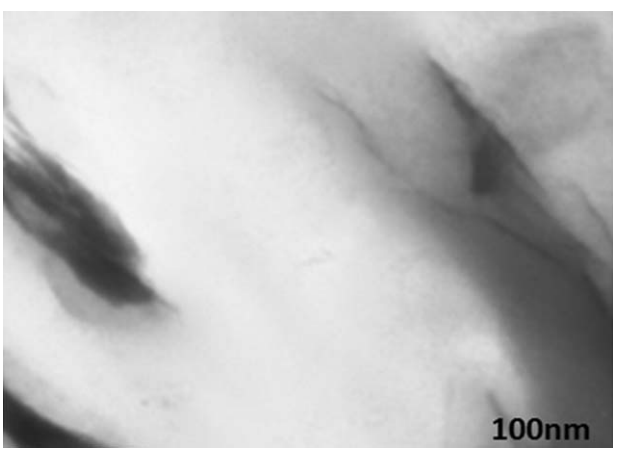

Figure 4 TEM image of PC + 3% OMMT-I nanocomposite.

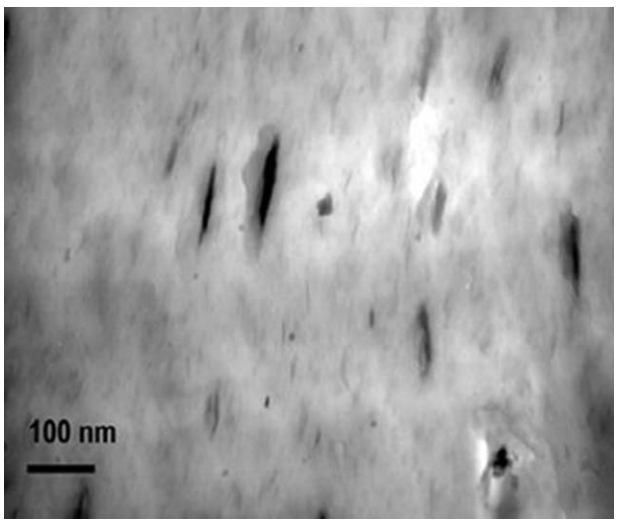

Figure 5 TEM images of PC + 3% Cloisite 20A nanocomposite.

indicating an exfoliated nanostructure as compared with Cloisite 20A and OMMT-I having particle aspect ratio of 42 and 33.7, respectively, results in intercalated nanomorphology. TEM micrograph of PC/Cloisite 15A reveals that most of the dispersed particles are thin tactoids contains several silicate layers with few single platelets and the exfoliated platelets are well aligned in the flow direction.

Thermal properties

Differential scanning calorimetry

Glass transition temperature (T_g) of neat PC and the nanocomposites detected from the DSC heating curve were represented in Figure 7. It was observed that PC and its nanocomposites showed only second-order transition, which is related to T_g. However, the absence of first transition gives a clear evidence of the absence of melting temperature, which

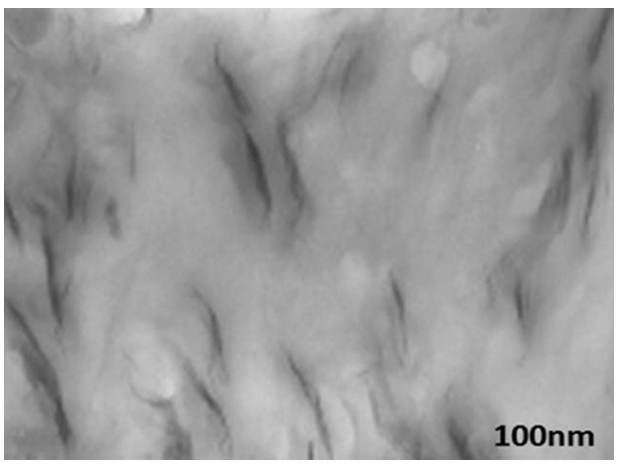

Figure 6 TEM images of PC + 3% Cloisite 15A nanocomposite.

TABLE III
Average Nanoparticle Dimensions in Nanocomposites Determined from TEM Analysis

Nanoclays	Average length (nm) = l	Average thickness (nm) = t	Average aspect ratio (l/t)
Na^+-MMT	700 ± 5.32	24 ± 1.26	29 ± 1.20
OMMT-I	472 ± 3.11	13 ± 0.83	36 ± 1.11
Cloisite 20A	210 ± 2.50	5 ± 0.10	42 ± 1.20
Cloisite 15A	162 ± 1.10	3 ± 0.10	54 ± 1.23

± indicates standard deviation which has been determined form the three tested samples.

TABLE IV
Effect of Nanoclay on the T_g of PC

Sample	T_g (°C)
PC (V)	148 ± 1.22
PC+3% Na^+-MMT	146 ± 1.15
PC+3% OMMT-I	151 ± 1.20
PC+3% Cloisite 20A	153 ± 1.11
PC+3% Cloisite 15A	158 ± 1.11

± indicates standard deviation which has been determined form the three tested samples.

was due to the amorphous nature of the polymer. The T_g value of PC, PC/Na^+-MMT, PC/OMMT-I, PC/Cloisite 20A, and PC/Cloisite 15A nanocomposites were shown in Table IV. It is seen from the Table IV that the T_g of PC (148°C) decreased by 2°C with incorporation of Na^+-MMT clay. This is mainly due to the absence of attractive interaction between the PC matrix and the natural montmorillonite having no organic functional groups. In case of PC/OMMT-I and PC/Cloisite 20A, there is an increase in T_g by 3°C and 5°C, respectively, as compared with PC indicating the compatibility of OMMT-I and Cloisite 20A with PC matrix. However, in case of PC/Cloisite 15A nanocomposites, there was a significant increase in the T_g by 10°C, 12°C, 7°C, and 5°C as compared to virgin PC, PC/Na^+-MMT, PC/OMMT-I, and PC/Cloisite 20A nanocomposites. This behavior of PC/Cloisite 15A is mostly due to higher compatibility of Cloisite 15A, which decreases the movement of PC chain segment effectively and increases T_g. The organic modifiers present in the organoclays enhance the interaction between PC and the organoclays that leads to an increase in glass transition. However, in case of PC/Na^+-MMT, the absence of attractive interaction between PC and Na^+-MMT having no functional group results in a slight decrease in T_g.

Thermogravimetric analysis

Thermal degradation behavior of PC and the nanocomposites are depicted in Figure 8 whereas Table V summarizes the degradation temperature at 5 wt % loss (T_{onset}), 50 wt % loss ($T_{0.5}$), and weight loss above 90% (T_{end}) of PC and the nanocomposites. It is obvious that regardless of the types of the organoclays, the thermal stability of all the nanocomposites increases. The improvement of thermal stability of the nanocomposites can be attributed to the shielding effect of clays. Small molecules generated during the thermal decomposition process cannot permeate but have to bypass claylayers.Thus, the addition of organoclays slows down the release rate of decomposed byproducts and enhances the thermal stability of the nanocomposites.[59] Furthermore, confinement of PC segments within the clay galleries also tends to retard the segmental motion of the matrix chains resulting in higher thermal stability. Values in Table

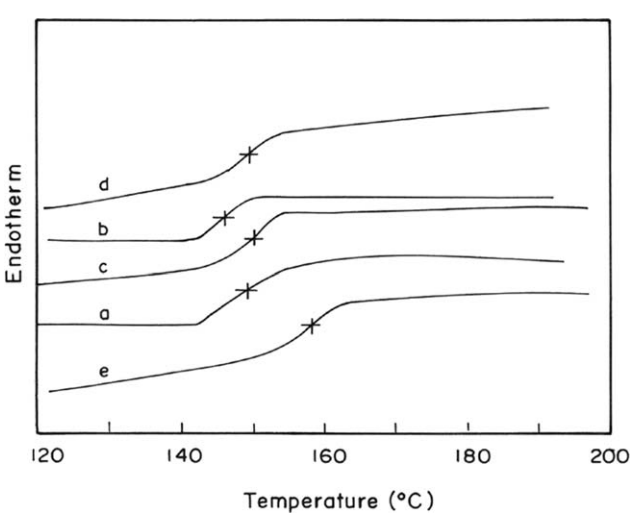

Figure 7 DSC thermograms of (a) PC (V), (b) PC/Na^+-MMT, (c) PC/OMMT-I, (d) PC/Cloisite 20A, (e) PC/Cloisite 15A nanocomposites.

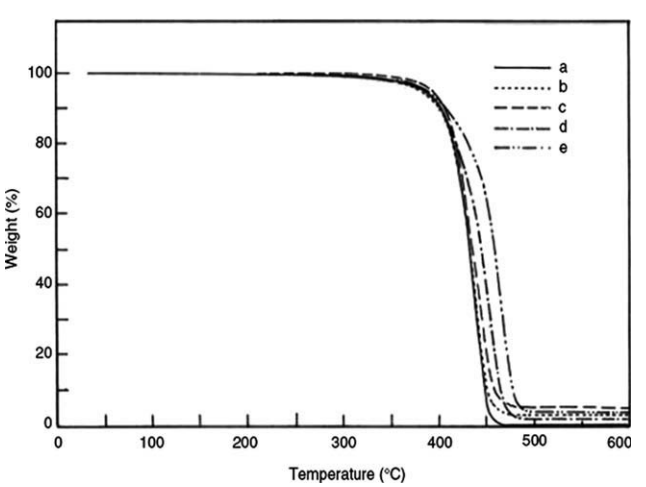

Figure 8 TGA thermograms of (a) PC (V), (b) PC/Na^+-MMT, (c) PC/OMMT-I, (d) PC/Cloisite 20A, (e) PC/Cloisite 15A nanocomposites.

TABLE V
Effect of Nanoclay on the Thermal Stability of PC

Sample	T_{onset} (°C)	$T_{0.5}$ (°C)	T_{end} (°C)	Residue (wt %)
PC (V)	390 ± 1.20	423 ± 1.12	460 ± 1.32	2 ± 0.10
PC+3% Na^+-MMT	392 ± 1.11	434 ± 1.30	463 ± 1.14	5 ± 0.13
PC+3% OMMT-I	396 ± 1.23	442 ± 1.12	473 ± 1.25	10 ± 0.28
PC+3% Cloisite 20A	410 ± 1.11	450 ± 1.16	481 ± 1.21	4 ± 0.13
PC+3% Cloisite 15A	416 ± 1.12	462 ± 1.11	490 ± 1.21	7 ± 0.24

± indicates standard deviation which has been determined form the three tested samples.

V revealed that the onset temperature of thermal degradation (T_{onset}) increases by a magnitude around 2 to 26°C by the addition of clays to the polymer matrix. T_{onset} for the PC/Na^+-MMT nanocomposites increased by 2°C only which is very close to that of PC whereas T_{onset} is increased by 100°C, 20°C, and 26°C in case of PC/OMMT-I, PC/Cloisite 20A, and PC/Cloisite 15A, respectively. Higher T_{onset} of nanocomposites with Cloisite 15A and Cloisite 20A nanoclay might be due to the presence of ditallow organic modifier with two methyl groups in Cloisite15A and Cloisite 20A.

The final degradation temperature (where the polymer degraded slightly greater than 90% in case of nanocomposites and close to 100% in case of virgin matrix) was almost same when PC was compared with PC/Na^+-MMT nanocomposite. This is due to the shielding of intercalated polymer chains by the confining clay layers, which did not occur in case of nanocomposites. This results also in coincidence with the results obtained from XRD, where no intercalation was evident in case of PC/Na^+-MMT nanocomposites. However, PC/Cloisite 15A nanocomposites possess higher thermal stability than others. This can be ascribed to the strong interaction between PC and Cloisite 15A and the higher dispersion of Cloisite 15A in the PC matrix in comparison with the other two organoclays.

Heat distortion temperature (HDT)

The HDT values of the PC and PC/Clay nanocomposites as shown in Table VI indicates an increase in HDT value with the addition of Na^+-MMT by 9°C as compared with pure PC (132°C), which further corroborated the higher thermal stability of the nanocomposites. However, with the incorporation of organomodified nanoclays (Cloisite 15A, Cloisite 20A, and OMMT-I), HDT values increases more significantly as compared to Na^+-MMT. Cloisite 15A reinforced PC nanocomposite shows an optimum HDT value of 170°C which is 38°C more than the HDT of pure PC. This reflects a higher exfoliation level of the organomodified nanoclay.[60]

Dynamic mechanical properties

Storage modulus (E')

The elastic modulus (E') is a measure of load bearing capacity of a material and is analogous to the flexural modulus, determined in accordance with ASTM D 790. Figure 9 illustrates the temperature dependence of storage modulus at 1 Hz for the virgin PC and nanocomposites with various organoclay. As expected, storage modulus (E') for the nanocomposites is higher than that of the neat PC in the whole range of testing temperature. It was found that the addition of nanoclays increases in modulus of virgin matrix and prominent in both glassy and rubbery regions. This may be due to the reinforcing effect imparted by nanoclays along with high aspect ratio of the clay platelets allowing a greater degree of stress transfer at the interface.[61] Furthermore, restricted segmental motion at organic-inorganic interface due to interaction of functionalized clay surface with PC matrix and exfoliation of clay galleries at the nanoscale level may be the possible cause for a phenomenal increase in the storage modulus. The improvement in storage modulus of the nanocomposites may also be caused by the stiffness of clay layers. It can be found that E' of the nanocomposites are significantly higher than that of PC up to 100°C and E' of PC/Cloisite 15A is optimum between −15 and 110°C. In addition, E' for PC/Na^+-MMT, PC/Cloisite 20A, and PC/Cloisite 15A nanocomposites remain constant or have slight increase when the temperature is beyond 50–100°C. However, the storage modulus of nanocomposites as well as the virgin PC decreases with increase in temperature. The rate of decrease in E' is more prominent upto −75°C and

TABLE VI
HDT of PC and PC Nanocomposites

Sample type	HDT (°C)
PC (Virgin)	132 ± 1.20
PC/3%Na^+-MMT	141 ± 2.30
PP/3% OMMT-I	150 ± 1.30
PP/3% Cloisite 20A	161 ± 1.50
PP/3% Cloisite 15A	170 ± 1.16

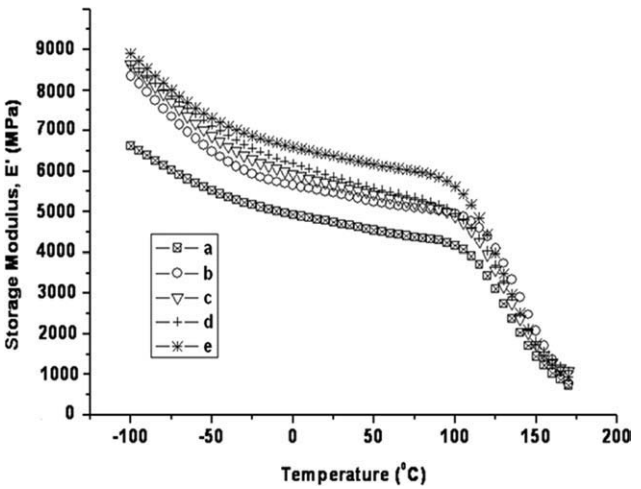

Figure 9 Storage modulus curve of (a) PC (V), (b) PC/Na^+-MMT, (c) PC/OMMT-I, (d) PC/Cloisite 20A, (e) PC/Cloisite 15A.

then becomes almost steady up to 120°C, after which the rate of decrease in E' further increases more significantly. A comparatively higher value of E' was obtained in case of PC nanocomposites with 3 wt % of Cloisite 15A due to the exfoliation of the clay layers leading to efficient dispersion of clay platelets throughout the interface regions of the nanocomposites thus decreasing the chain mobility when periodic load was applied.

Loss modulus (E'')

Loss modulus curve for virgin PC, Na^+-MMT, and treated clay (OMMT-I, Cloisite 20A, Cloisite 15A) nanocomposite was shown in the Figure 10. Figure 10 shows an increase in loss modulus for nanocomposites as compared with virgin PC. The nanocomposite with Cloisite 20A shows higher loss modulus as compared with other nanocomposites in the order of PC/Na^+-MMT < PC/OMMT-I < PC/Cloisite 20A < PC/Cloisite 15A. In addition to the increase in loss modulus, the loss modulus peaks which correspond to the glass transition temperature are also shifted to higher temperature as a function clay type. The shifting of loss modulus peak toward higher temperature for the nanocomposites is attributed to the enhancement of a restricted mobility of the interphase region. Further, the highest loss modulus of the PC/Cloisite 15A nanocomposites indicates the greater dispersibility with matrix. However, a point of great interest is the broadening of the loss modulus peak at T_g or above T_g for organomodified nanocomposites can be explained by the increased interaction of PC matrix with surface-modified nanoclays.

Damping factor (tan δ)

The variation of damping factor (tan δ) with temperature was presented in Figure 11. The tan δ curve represents the ratio of dissipated energy to storage energy. The glass transition temperature (T_g) of the virgin matrix as well as the nanocomposites was determined from the peak value of tan δ curve. The virgin matrix exhibited glass transition temperature around 145°C that increased with the incorporation of both organomodified nanoclays. The reason for the enhancement in T_g may be due to restricted mobility of confined chain in an intercalated/exfoliated system in case of treated clay nanocomposites. Thus, the damping value increases due to incorporation of inorganic clay platelets or the nanocomposites. A small decrease in T_g of PC/Na^+-MMT nanocomposite is observed which is attributed to the weak interaction at the interface region of the

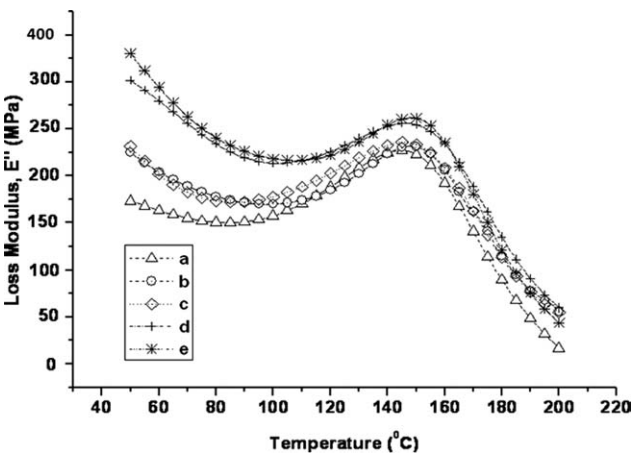

Figure 10 Loss modulus curve of (a) PC (V), (b) PC/Na^+-MMT, (c) PC/OMMT-I, (d) PC/Cloisite 20A, (e) PC/Cloisite 15A.

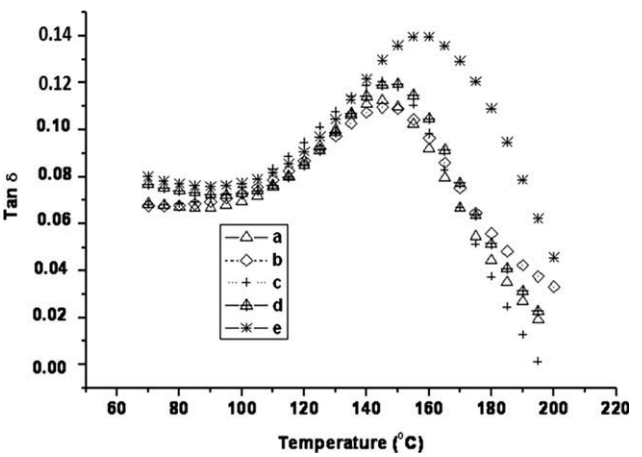

Figure 11 Damping factor curve of (a) PC (V), (b) PC/Na^+-MMT, (c) PC/OMMT-I, (d) PC/Cloisite 20A, (e) PC/Cloisite 15A.

nanocomposites due to the absence of surface modification on Na^+-MMT. Therefore, the mobility of PC polymer chain in the PC/Na^+-MMT nanocomposites at the interface is more than that of in virgin PC. However, the shifting tan δ peak toward higher temperature with the inclusion of surface modified nanoclays indicates an increase in T_g which further resembles the observation obtained from DSC analysis. This is ascribed to the confinement of intercalated PC chains within the silicate galleries that prevents the segmental motions of the polymer chains and leads to an increase in T_g. The interaction between the organoclay and the PC molecules may create an interfacial zone of polymer with reduced mobility. This reduced mobility material, in turn, causes an increase in the T_g composite. However, with the strong interaction Cloisite 15A with PC will further hamper the dynamics of the polymer chains, hindering segmental motion and thus leads to the higher T_g for PC/Cloisite15A nanocomposites than others.

CONCLUSION

PC nanocomposites with different type of nanoclays were successfully fabricated by using direct melt compounding technique. The experimental findings revealed that organic modification of Na^+-MMT with quaternary ammonium surfactants, i.e., OMMT-I and commercially available organoclays resulted in improved dispersion of the nanoclays with intercalated/exfoliated nanomorphology. Mechanical tests reveal an optimum mechanical performance of PC nanocomposites with 3 wt % of Cloisite 15A. The glass transition temperature and thermal stability of the PC increased in the organomodified-based PC nanocomposites suggesting confinement of PC segments within the clay galleries that tends to retard the segmental motion of the matrix chains. PC nanocomposites prepared using Cloisite 15A significantly promotes mechanical strength and modulus thus confirming higher dispersibility and increased interfacial adhesion within the polymer matrix. PC/OMMT-I nanocomposites also exhibited improved performance characteristics as compared with the nanocomposites prepared using Na^+-MMT nanoclay. Morphological studies reveal that the dispersion of nanoclay in the matrix depends on the surfactant used in the organoclay.

References

1. Giannelis, E. P. Adv Mater 2004, 8, 29.
2. Wang, Z.; Pinnavaia, T. S. Chem Mater 1998, 10, 1820.
3. Burnside, S. D.; Giannelis, E. P. Chem Mater 1995, 7, 1597.
4. Alexandre, M.; Dubois, P. Mater Sci Eng 2000, 28, 1.
5. Gilman, J. W. Appl Clay Sci 1999, 15, 31.
6. Gilman, J. W.; Kashiwagi, T.; Nyden, M.; Brown, J. E. T.; Jackson, C. L.; Lomakin, S.; Giannelis, E. P.; Manias, E. Chemistry and Technology of Polymer Additives; Royal Society of Chemistry: England, Cambridge, 1999; p 249.
7. Gilman, J. W.; Jackson, C. L.; Morgan, A. B.; Harris, J. R.; Manias, E.; Giannelis, E. P.; Wuthenow, M.; Hilton, D.; Phillips, S. H. Chem Mater 2000, 12, 1866.
8. Giannelis, E. P.; Krishnamoorthi, R.; Manias, E. Adv Polym Sci 1999, 138, 107.
9. Le Barron, P. C.; Wang, Z.; Pinnavaia, T. J. Appl Clay Sci 1999, 15, 11.
10. Ray, S. S.; Okamoto, M. Prog Polym Sci 2003, 28, 1539.
11. Krishnamoorthi, R.; Vaia, R. A.; Giannelis, E. P. Chem Mater 1996, 8, 1728.
12. Wang, Y.; Chen, F. B.; Li, Y. C.; Wu, K. C. Compos Part B: Eng 2004, 35, 111.
13. Yilmazer, U.; Ozden, G. Polym Compos 2006, 27, 249.
14. Cho, J. W.; Paul, D. R. Polymer 2001, 42, 1083.
15. Fornes, T. D.; Hunter, D. L.; Paul, D. R. Macromolecules 2004, 37, 1793.
16. Wu, Z.; Zhou, C.; Zhu, N. Polym Test 2002, 21, 479.
17. Tyan, H. L.; Liu, Y. C.; Wei, K. H. Polymer 1999, 40, 4877.
18. Ma, J.; Zhang, S.; Qi, Z. N. J Appl Polym Sci 2001, 82, 1444.
19. Acierno, D.; Scarfato, P.; Amendola, E.; Nocerino, G.; Costa, G. Polym Eng Sci 2004, 44, 1012.
20. Kawasumi, M.; Hasegawa, N.; Kato, M.; Usuki, A.; Okada, A. Macromolecules 1997, 30, 6333.
21. Usuki, A.; Kato, M.; Okada, A.; Kurauchi, T. J Appl Polym Sci 1997, 63, 137.
22. Hasegawa, N.; Okamoto, H.; Kato, A.; Usuki, M. J Appl Polym Sci 2000, 78, 1918.
23. Huang, X.; Brittain, W. J. Macromolecules 2001, 34, 3255.
24. Chen, G.; Chen, X.; Lin, Z.; Ye, W.; Yao, K. J Mater Sci Lett 1999, 18, 1761.
25. Yang, H. H.; Sung, T. L.; Hyoung, J. C.; Myung, S. J. Macromolecules 2001, 34, 8084.
26. Wanjale, S. D.; Jog, J. P. J Appl Polym Sci 2003, 90, 3233.
27. Xu, W.; Ge, M.; He, P. J Appl Polym Sci 2001, 82, 2281.
28. Balakrishnan, S.; Neelakantan, N. R.; Jaisankar, S. N. J Appl Polym Sci 1999, 74, 2102.
29. Lee, L. J Polym Sci Part A 1964, 2, 2859.
30. Mishra, S. P.; Venkidusamy, P. J Appl Polym Sci 2003, 58, 2229.
31. Riga, A.; Collins, R.; Mlachak, G. Thermochim Acta 1998, 324, 135.
32. Davis, A. Die Makromol Chem 2003, 132, 23.
33. Bratosiewicz, R. L.; Booth, C. Eur Polym J 1974, 10, 791.
34. Abbas, K. B. Polymer 1980, 21, 936.
35. Abbas, K. B. Polymer 1981, 22, 836.
36. Le Grand, D. G.; Bendler, J. T. Handbook of Polycarbonate Science and Technology; Marcel Dekker: New York, 2000.
37. Dong, L. S.; Greco, R.; Orsello, G. Polymer 1993, 34, 1375.
38. Quentens, D.; Groeninckx, G.; Guest, M.; Aerts, L. Polym Eng Sci 1991, 31, 1207.
39. Kang, E. A.; Kim, J. H.; Kim, C. K.; Rhee, H. W.; Oh, S. Y. Polym Eng Sci 2000, 40, 2374.
40. Kim, J. H.; Kim, C. K. J Appl Polym Sci 2003, 89, 2649.
41. Seo, Y. S.; Kim, J. H.; Kim, C. K.; Lee, R.; Keum, J. K. J Appl Polym Sci 2005, 96, 2097.
42. Tan, C. S.; Kuo, T. W. J Appl Polym Sci 2005, 98, 750.
43. Zhaobo, W.; Xie, G.; Wang, X.; Li, G.; Zhang, Z. Mater Lett 2006, 60, 1035.
44. Huang, X.; Lewis, S.; Brittain, W. J. Macromolecules 2000, 33, 2000.
45. Severe, G.; Hsieh, A. J.; Koene, B. E. SPE ANTEC 2000, 2, 1523.

46. Yoon, P. J.; Hunter, D. L.; Paul, D. R. Polymer 2003, 44, 5323.
47. Lee, K. M.; Han, C. D. Polymer 2003, 44, 4573.
48. Jisheng, M. A.; Zongneng, Q. I.; Youliang, H. U. J Appl Polym Sci 2001, 82, 3611.
49. Liu, X.; Wu, Q.; Berglund, L. A.; Lindberg, H.; Fan, J.; Qi, Z. J Appl Polym Sci 2003, 88, 953.
50. Miyagawa, H.; Michael, J. R.; Lawrence, T. D. Polym Compos 2004, 26, 42.
51. David, A. U.S. pat. US2008/0064798 A1 (2008).
52. Rong, M. Z.; Zhang, M. Q.; Zhang, Y. X.; Zeng, H. M.; Watter, R.; Friedrich, K. Polymer 2001, 42, 167.
53. Dasari, A.; Lim, S. H.; Yu, Z. Z.; Mai, Y. W. Aust J Chem 2007, 60, 496.
54. Alexandre, M.; Beyer, G.; Henrish, C.; Cloots, R.; Rulmont, A.; Jerome, R.; Dubois, P. Macromol Rapid Commun 2001, 22, 643.
55. Huang, J. C.; Zhu, Z. K.; Ma, X. D.; Qian, X. F.; Yin, J. J Mater Sci 2001, 36, 871.
56. Shah, D.; Maiti, P.; Jiang, D.; Batt, C. A.; Giannelis, E. P. Adv Matter 2005, 17, 525.
57. Mert, M.; Yilmazer, U. J Appl Polym Sci 2008, 108, 3890.
58. Dasari, A.; Yu, Z. Z.; Mai, Y. W.; Hu, G. H.; Varlet, J. Compos Sci Technol 2005, 65, 2314.
59. Liu, Z.; Chen, K.; Yan, D. Polym Test 2004, 23, 323.
60. Singh, A. U.S. Pat. 6,057,035 (2000).
61. Hasegawa, N.; Okamoto, H.; Kawaswami, M.; Usuki, A. J Appl Polym Sci 1999, 74, 3359.